Effects of wind and sea ice drift on the seasonal variation of warm circumpolar deep water in the Amundsen Sea

Tae-Wan Kim[1], Ho Kyung Ha[1,2], Anna K. Wåhlin[3], Jae Hak Lee[4], Hyun Jung Lee[1], Yang-Ki Cho[5] and SangHoon Lee[1]

[1]Korea Polar Research Institute, Incheon 406-840, South Korea ,[2]Department of Ocean Sciences, Inha University, Incheon 402-751, South Korea,[3]Department of Earth Sciences, University of Gothenburg, Gothenburg, Sweden
[4]Korea Institute of Ocean Science and Technology, Ansan 425-600, South Korea, [5]School of Earth and Environmental Sciences, Seoul National University, Seoul 151-742, South Korea

Korea Polar Research Institute

Introduction

The most rapidly changing region of the West Antarctic is the Amundsen Sea, where the intrusion of relatively warm circumpolar deep water (CDW) onto the continental shelf may help reduce ice thickness. Temporal variation in the flow of MCDW was examined using a mooring current meter in the center of the deep inflow in the Dotson Trough. On short-term (less than a week) scales, the velocity has strong barotropic fluctuations that correlate with the eastward wind at the shelf break. In addition to these short-term fluctuations, there is a persistent south-eastward baroclinic flow of dense warm water. Neither the baroclinic flow nor the bottom temperature could be shown to correlate with the wind from the time series. Furthermore, since the pronounced summertime maximum in warm layer thickness in Dotson Trough is not related to any maximum in the eastward winds, it is unlikely that eastward winds force the flow of MCDW into the Dotson Trough other than the short-term oscillations. The main objective of this study was to examine the combined effect of wind and sea ice drift on the on-shelf flow of CDW in the Amundsen Sea. In order to understand the effects of wind and sea ice on the seasonal variation in the thickness of MCDW, we calculate the ocean surface stress curl and Ekman pumping velocity in Amundsen Sea.

Oceanography survey

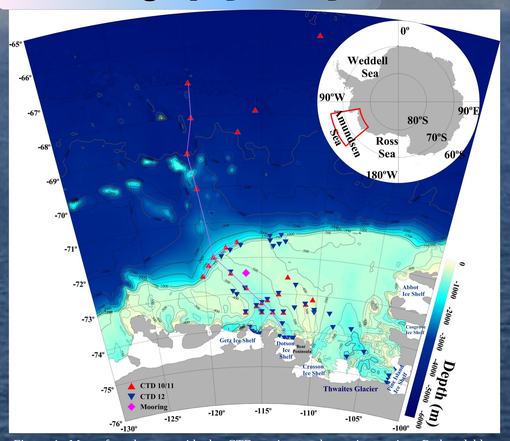

Figure 1. Map of study area with the CTD stations and mooring station. Red and blue triangles show the CTD stations during the 2010/11 and 2012 Araon expeditions, respectively. The purple diamond indicates the mooring station (February, 2010 to February, 2012).

Two oceanographic surveys were conducted by the IBRV Araon from 21 December 2010 to 23 January 2011, and from 31 January to 20 March 2012 (Figure 1). A total of 30 and 52 CTD stations were occupied during the surveys in 2011 and 2012, respectively. The temporal variability and properties of CDW were observed from a mooring (72.46°S, 116.35°W) in the eastern side of Dotson Trough (Figure 1) from 15 February 2010 to 1 March 2012.

The mooring line contained Microcats (Seabird, SBE-37SMP) to measure temperature (with an accuracy of 0.002 K) and conductivity (with an accuracy of 0.0003 S m^{-1}); 5 during the first observation period (15 February 2010 to 25 December 2010) and 7 during the second observation period (25 December 2010 – 1 March 2012). An upward-looking 150-kHz Acoustic Doppler Current Profiler (ADCP; RDI) was deployed at the bottom to measure current velocity profiles. The observed velocity data were processed using the WinADCP® software.

The measured velocity was de-tided using the t_tide toolbox for harmonic analysis. In order to calculate the Ekman pumping velocity, we use the reanalysis wind data and observed sea ice concentration and velocity data from satellite. Wind data were obtained from the ERA interim reanalysis data. Sea ice concentration data were obtained from the Nimbus-7 SMMR, DMSP, SSM/I, SSMIS. The sea ice velocity data were obtained from the Polar Pathfinder Daily 25 km EASE-Grid Sea Ice Motion Vectors Version 2 from 1990 to 2011.

Seasonal and temporal variation of the MCDW layer

The warmest (>2°C) water is found at about 300-500 m depth at 67°S (St. 29). This warm and salty tongue of CDW extends toward the ice shelf, becoming colder and fresher as it interacts with the surface water and/or subsurface contact with glacial ice. Near the coast, in MCDW, the observed maximum temperature was 0.7°C and the observed maximum salinity was 34.6 psu. In the sea ice covered stations (e.g., St. 07 and St. 08), surface temperatures were lower than that in northern limit of ice area. The thickness of the warm layer (identified here as T> 0°C isotherm) and the bottom temperature vary distinctly with season; both attain maxima in austral summer and minima in austral winter. The difference between the seasonal maximum and minimum in thickness is approximately 60-100m and the difference between maximum and minimum bottom temperature is approximately 1°C (0.25-1.2°C). In contrast to temperature and salinity, the seasonal variation of along-trough velocity (Figure 3d) is relatively weak. The velocity variability is dominated by barotropic fluctuations induced by the local wind (Wåhlin et al., 2013). However, the local wind is not significantly correlated with either warm layer thickness or bottom temperature (Wåhlin et al., 2013). Hence, the observed seasonal variation in temperature and salinity is not likely caused by the local wind. The time-series of the heat content mirrors the seasonal variation in the thickness of the MCDW layer. For vertically averaged heat content, the maximum exceeded 9.5 MJ m^{-3} in February 2011 and fell to roughly 4.1 MJ m^{-3} in December 2011. The mean-amplitude of the seasonal variation in vertically averaged heat content is about 2 MJ m^{-3}. The direction and magnitude of total stress was determined by the ocean surface wind vector at ice free area north of sea ice zone at whole seasons. However, at sea ice zone, the total stress decreased sharply towards the ice shelf compared with the wind stress and increased again at polynyas surface stress.

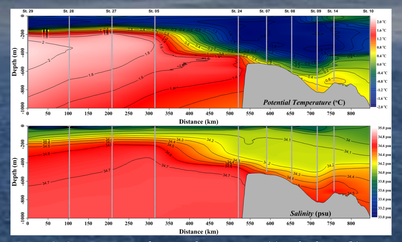

Figure 2. Cross sections of potential temperature (a) and salinity (b) along the transect from 67° S to Dotson Ice shelf.

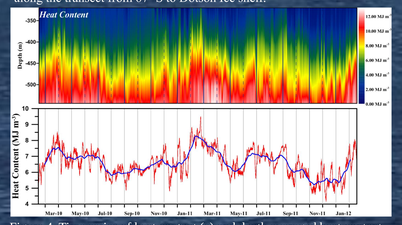

Figure 4. Time series of heat content (a) and depth averaged heat content (b). The blue line in (b) represents the 31-day moving average.

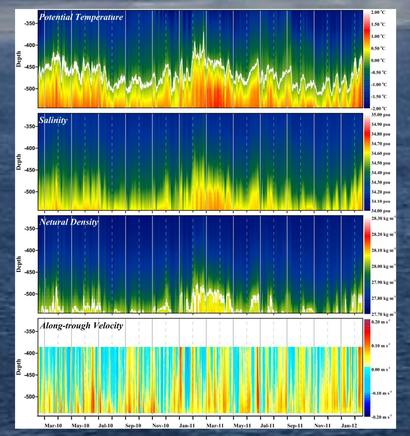

Figure 3. Time-series variation of potential temperature (a), salinity (b), neutral density (c) and along-trough velocity (d) at the mooring station. The white line in (a) indicates the upper boundary of the warm layer (0°C isotherm).

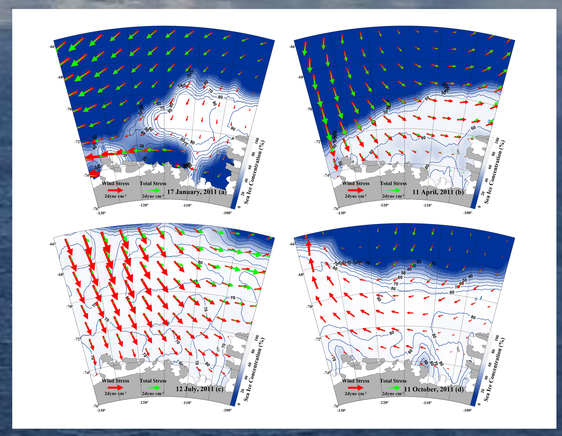

Figure 5. The snapshots of the wind stress (red arrow) and total stress (green arrow) and sea ice concentration on (a) January 17, (b) April 11, (c) July 12, and (d) October 11, 2011.

Spatial and temporal variation of the ocean surface stress

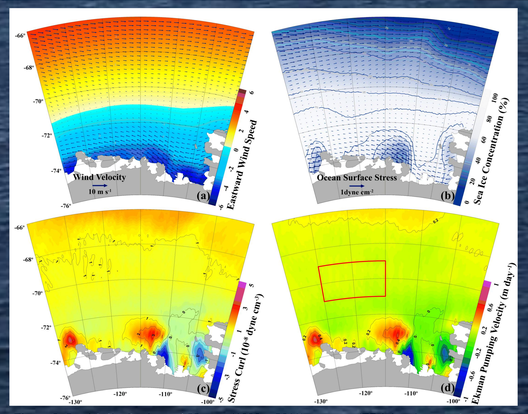

Figure 6. Spatial distributions of 22-year (1990 – 2011) averages (ERA interim reanalysis data) of (a) wind velocity, (b) ocean surface stress (blue arrow) and sea ice concentration, (c) stress curl, and (d) Ekman pumping velocity. The red rectangle in Figure 6d highlights the Amundsen Sea shelf break.

To examine the effects of the varying Ekman pumping velocity on the seasonality of both the heat content and the position of the 0°C isotherm, a time series of the wind field and the sea ice extent were used. Maximum eastward ocean surface stress (0.5 dyne cm^{-2}) was at 66°S, where the sea ice concentration was less than 0.25. The minimum absolute value of ocean surface stress (0.03 dyne cm^{-2}) was noted at the area of highest sea ice concentration (70°S). Stress curl and Ekman pumping velocity at the sea surface were calculated from the horizontal variation of ocean surface stress. An extensive area of positive wind stress curl and high Ekman pumping velocities (>0.26 m day^{-1}) was located around 66°S. Between 68°S and 71°S, where sea ice concentration is higher than 40%, the stress curl is less than 0.5×10^{-8} dyne cm^{-3}.

Wind stress curl and sea ice concentration, both of which show pronounced seasonal variation, give rise to spatial variation in the Ekman pumping velocity. From February to April (FMA), north of 70°S, Ekman pumping exceeds 0.2 m day^{-1} due to latitudinal variation in the sea ice concentration and the wind. North of 68°S, despite the latitudinal variation of wind, Ekman pumping velocity decreases due to the horizontally homogenous sea ice concentration. A strong Ekman pumping occurs near the Amundsen Sea shelf break. From August to October (ASO), the sea ice zone extends north of the shelf break and the Ekman pumping velocity at the shelf break is notably weak during this season.

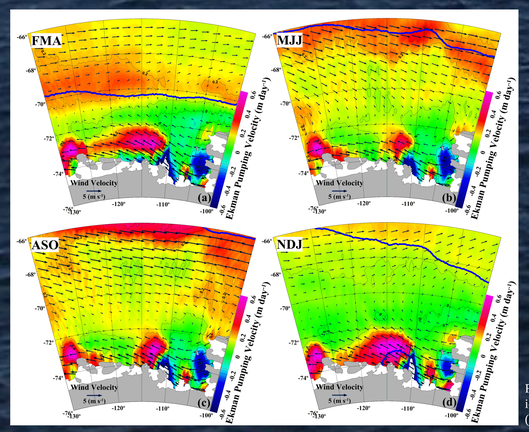

Figure 7. Spatial distributions of seasonal means of wind velocity (arrow), Ekman pumping velocity, and 20% sea ice concentration line (blue line), measured over a 22-year period (1990 – 2011) during (a) February-March-April, (b) May-June-July, (c) August-September-October, and (d) November-December-January.

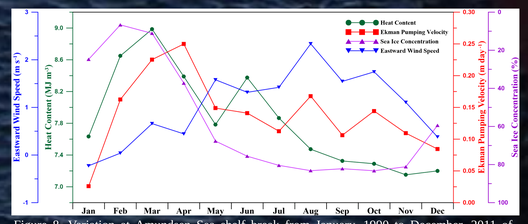

Figure 8. Variation at Amundsen Sea shelf break from January, 1990 to December, 2011 of monthly mean Ekman pumping velocity (red line), sea ice concentration (purple line), and eastward wind velocity (blue line); and variation in heat content (green) at the mooring station from 15 February, 2010 to 1 March, 2012.

Both heat content and the position of the 0°C isotherm showed seasonal variation, attaining a maximum during austral summer and a minimum during austral winter. The meridional variation in the observed isohalines and isotherms north of Amundsen Sea shelf break suggests that the thermocline depth depended mainly on the upwelling/downwelling caused by local wind patterns and sea ice conditions. Therefore, it appears that the seasonal variation of the thickness of the CDW at the Amundsen Sea shelf break is mainly affected by the variation in local wind patterns and sea ice condiztions. The monthly averaged sea ice concentration was less than 50% from January to April and higher than 50% for the rest of the year. The Ekman pumping velocity reached a maximum of 0.25 m day^{-1} in April when the sea ice concentration was less than 40% and the marginal ice zone was located at Amundsen Sea shelf break. In the austral winter, the sea ice concentration was high (> 80%) and latitudinally homogenous at the Amundsen Sea shelf break; so the Ekman pumping was small, even though the eastward wind was stronger.

Discussion and conclusions

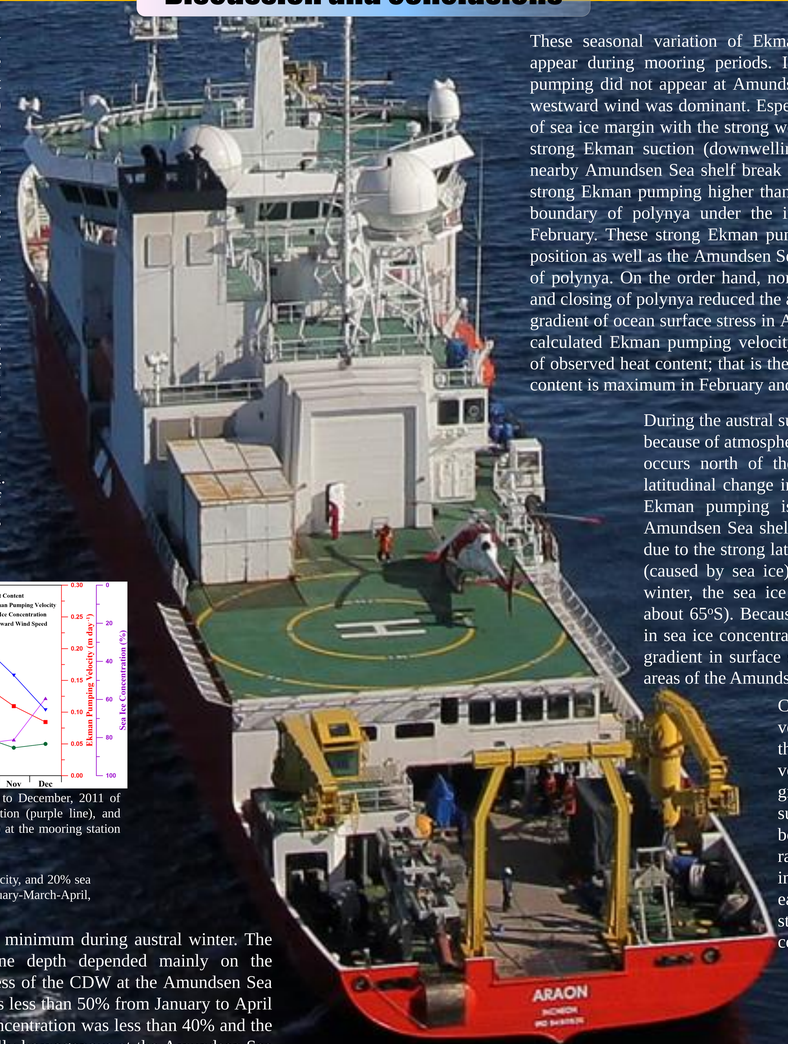

These seasonal variation of Ekman pumping velocity was also appear during mooring periods. In February, the strong Ekman pumping did not appear at Amundsen Sea shelf break because the westward wind was dominant. Especially, the southward movement of sea ice margin with the strong westward winds has generated the strong Ekman suction (downwelling) at south of sea ice margin nearby Amundsen Sea shelf break in February, 2011. However the strong Ekman pumping higher than 0.5 m day^{-1} appear at northern boundary of polynya under the influence of westward wind in February. These strong Ekman pumping influence to the mooring position as well as the Amundsen Sea shelf break with the extension of polynya. On the order hand, northern extension of sea ice zone and closing of polynya reduced the absolute magnitude of latitudinal gradient of ocean surface stress in August. The monthly variation of calculated Ekman pumping velocity corresponded well with those of observed heat content; that is the both Ekmam pumping and heat content is maximum in February and minimum in August.

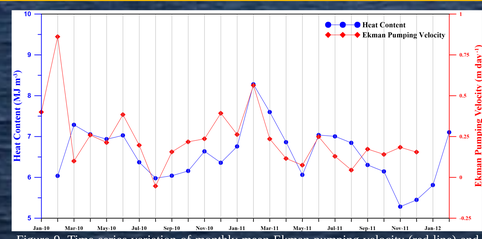

Figure 9. Time series variation of monthly mean Ekman pumping velocity (red line) and heat content (blue line) at the mooring station from January, 2010 to February, 2012.

During the austral summer, the sea ice zone contracts because of atmospheric heating, and Ekman pumping occurs north of the sea ice boundary due to the latitudinal change in velocity of the eastward wind. Ekman pumping is especially strong around the Amundsen Sea shelf break or sea ice marginal zone due to the strong latitudinal gradient in surface stress (caused by sea ice). In contrast, during the austral winter, the sea ice zone extends further north (to about 65ºS). Because of the horizontal homogeneity in sea ice concentration, there is less of a latitudinal gradient in surface stress across the sea ice covered areas of the Amundsen Sea shelf.

Consequently, Ekman pumping velocity is also lower, although the latitudinal change in wind velocity in austral winter is greater than that in austral summer. Around the sea ice boundary, however, there is a rather large latitudinal difference in wind stress, due to the strong eastward wind speed and the steep latitudinal change in sea ice concentration

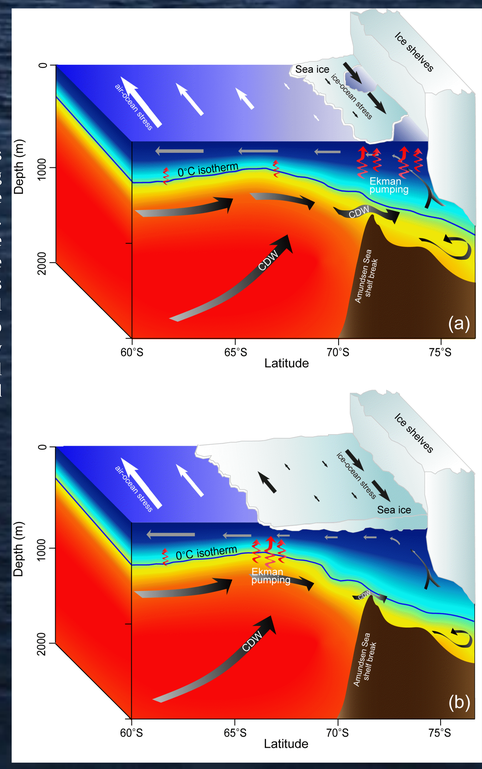

Figure 10. Schematic diagrams explaining the circulation of deep warm water and glacier meltwater and their relationship with wind forcing and sea ice distribution during austral summer (a) and winter (b) in the Amundsen Sea.